

Maintenance of the International Celestial Reference Frame

S. Lambert, E. F. Arias

SYRTE, Observatoire de Paris, Université PSL, CNRS, Sorbonne Université, LNE
61 av. de l'Observatoire, 75014 Paris, France

Published in IERS annual report 2020-23

1. The international reference frame ICRF3

Resolution B2 of the XXX IAU General Assembly (IAU 2019) resolves that as from 1 January 2019 ICRF3 is the fundamental realization of the International Celestial Reference System (ICRS). This third representation of the ICRS in radio wavelengths is a catalog of radio source positions described in Charlot et al. (2020) and consists of three catalogs at bands S/X, K and X/Ka with 4536, 824 and 678 objects respectively [<http://iers.obspm.fr/icrs-pc/newwww/icrf>]. Objects in the new frame had been used to orientate the second and third Gaia (Prusti et al. 2016, Brown et al. 2016) data releases DR2 (Brown et al. 2018, Mignard et al. 2018) and EDR3 (Brown et al. 2021, Klioner et al. 2022) catalogs onto the ICRS, as will be the case of the Gaia future catalog releases.

2. Monitoring of the ICRS

Monitoring the ICRS is a mission of the IERS ICRS Centre. With this aim, we perform on a regular basis verification of the stability of the axes of the system materialized through the frame, we characterize the possible deformations of the frame and track the astrometric evolution of its defining sources. Another aspect of this activity consists on the analysis of individual solutions, most of them submitted by the VLBI analysis centres to the International VLBI Service (IVS), and their comparison with the international references.

The IERS ICRS Centre at Paris Observatory developed the tools for determining the orientation of the axes, characterizing the deformations of the frame and analyzing the astrometric quality of radio source positions (Lambert & Malkin 2023). We present in this report analyses with respect to the conventional reference ICRF3, as well as with respect to Gaia Early Data Release 3 catalog (EDR3).

3. Analysis of recent VLBI catalogs

3.1. Data

We analyzed eight catalogs computed by seven IVS analysis centres in 2022, 2023 and 2024. The catalogs were respectively computed by the Space Geodesy Centre of the Italian Space Agency (ASI/CGS; solution asi2022a), Geoscience Australia (solution aus2024a), the German Federal Agency for Cartography and Geodesy (BKG; solution bkg2023b), the Geospatial Information Authority of Japan (GSI; solution gsi2023b), the Paris Observatory (OP; solution opa2023a), the United States Naval Observatory (USNO; solution usn2024a), and the Vienna Center for VLBI (VIE; solutions

2022sx and 2022vg). The solutions from ASI, BKG, GSI, OPA and USNO were obtained with Calc/Solve (Ma et al. 1986). The solution from AUS was obtained with the OCCAM geodetic VLBI analysis software package (Titov et al. 2004); the solutions from VIE were obtained with the Vienna VLBI Software VieVS (Boehm et al. 2018).

The individual frames of all the catalogs had been oriented on ICRF3 by applying no net rotation constraints on ICRF3 defining sources, loose in AUS and OPA solutions. Positions in ICRF3 had been adopted for the a priori catalogs in all the solutions included in this analysis; a priori positions for new sources in OPA come from the data base content. Right ascensions and declinations have been computed as global parameters in all solutions.

The galactocentric aberration has been corrected according to MacMillan et al. (2019) and to the recommendation of the IVS Working Group on Galactic Aberration.

In our analysis we have compared these individual solutions to the catalog representing ICRF3 in the S/X bands (ICRF3X in this report) and to the catalogue resulting from the Gaia Early Data Release 3 (EDR3, Prusti et al. 2016, Brown et al. 2021).

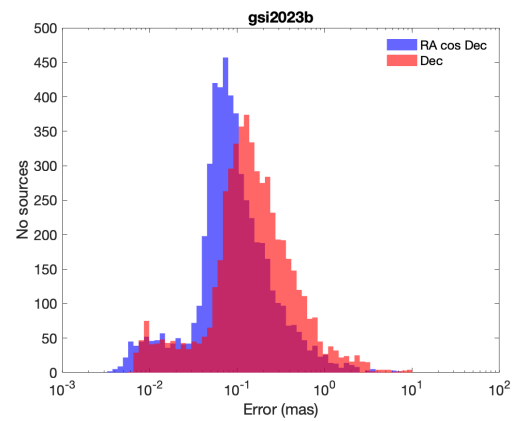
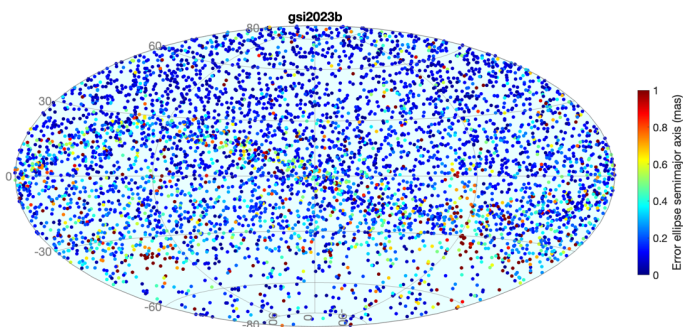
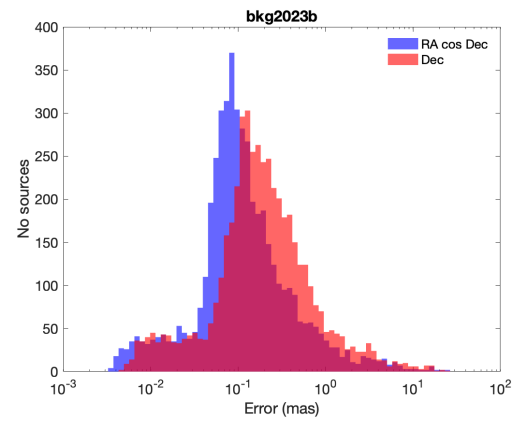
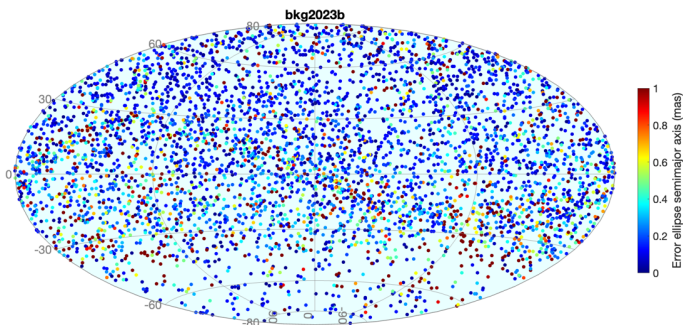
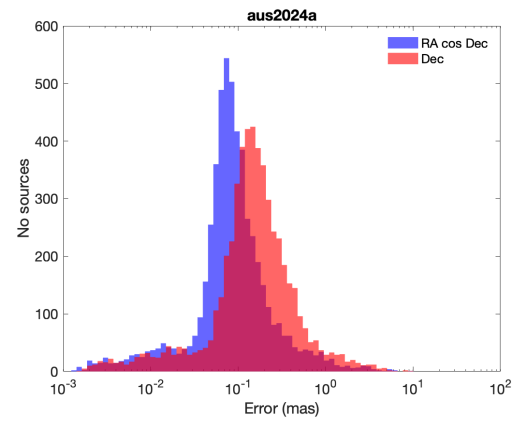
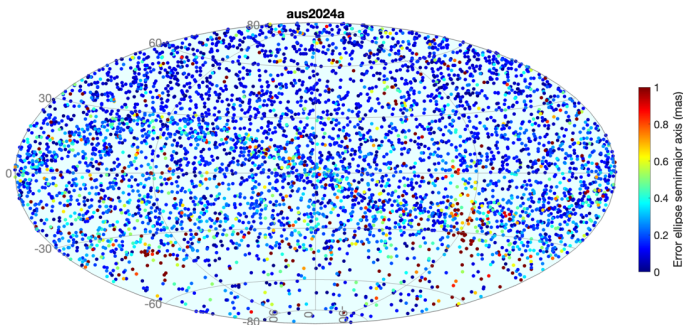
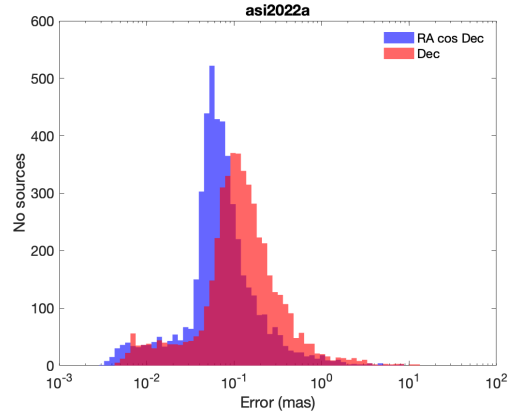
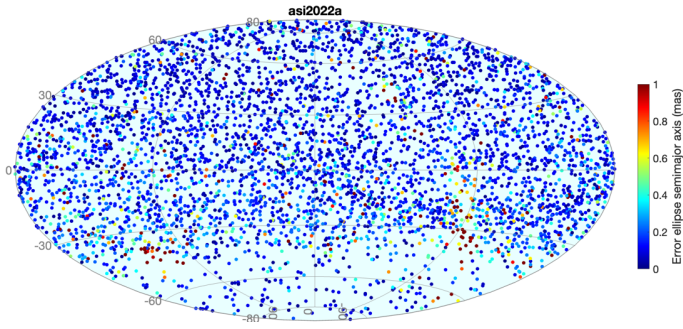
3.2. Overview of the catalogs

The number of sources in each catalog, the mean epoch of the observations, and the median positional errors (for RA cos DEC, Dec, and for the error ellipse major axis) are reported in Table 1. The standard error of the catalog positions reasonably differs in the solutions.

The sky distribution of the radio sources in each catalog is plotted in Fig. 1 together with the distribution of the standard errors. In the sky maps, the color indicates the overall error computed as the major axis of the error ellipse, calculated using the correlation information between the coordinates as provided in the catalogs.

Table 1. *Statistic information of the catalogs here reported. N is the number of sources. The mean epoch corresponds to the average of the mean observational epochs of each source. N is the number of sources, E_RA*, E_Dec are respectively the median standard errors in right ascension (scaled by cos dec) and in declination, E_EEMA is the median standard error along the major axis of error ellipses. Unit is μ as.*

	N	Epoch mjd	E_RA* uas	E_Dec uas	E_EEMA uas
asi2022a	4791	57610.77	65.79	115.50	117.65
aus2024a	5428	57733.30	81.77	148.70	152.10
bkg2023b	4842	57376.50	99.36	174.85	181.06
gsi2023b	5384	57708.75	82.73	143.90	146.72
opa2023a	4619	56099.30	123.51	207.10	217.92
usn2024a	5639	57780.90	108.43	189.40	193.21
vie2022sx	5423	57702.70	143.02	248.70	253.20
vie2022vg	5423	57707.80	142.33	247.40	251.90



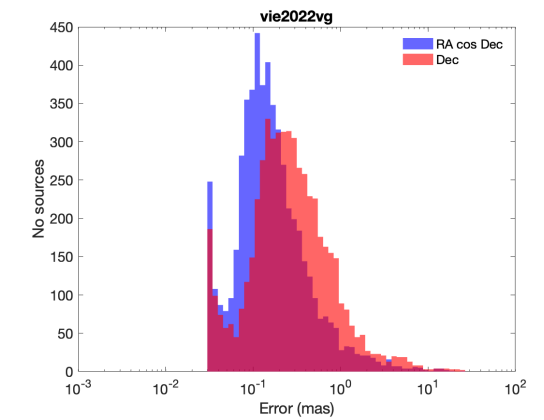
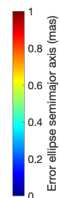
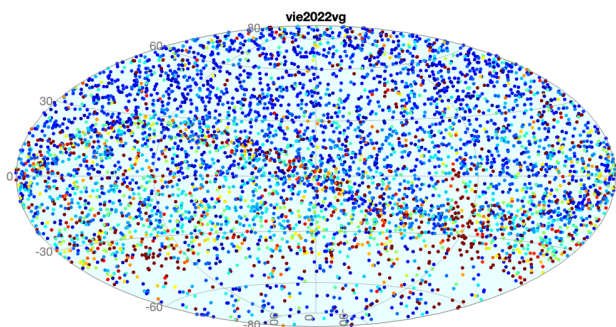
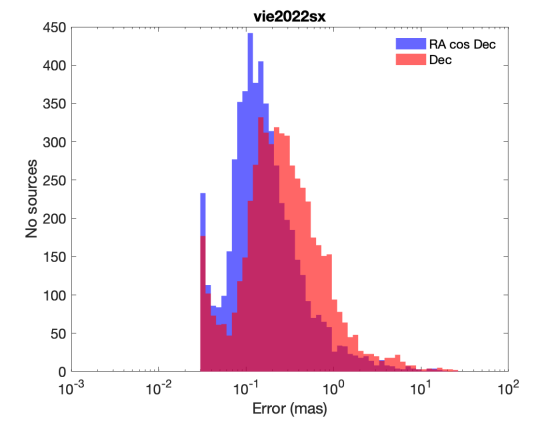
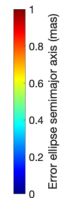
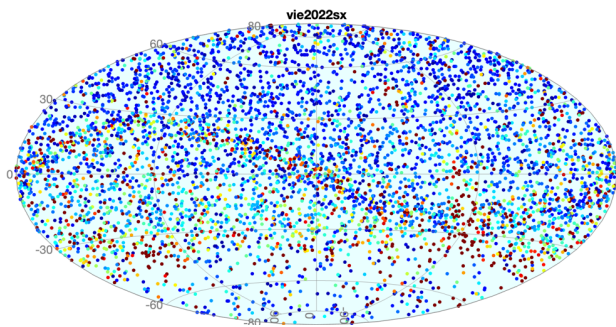
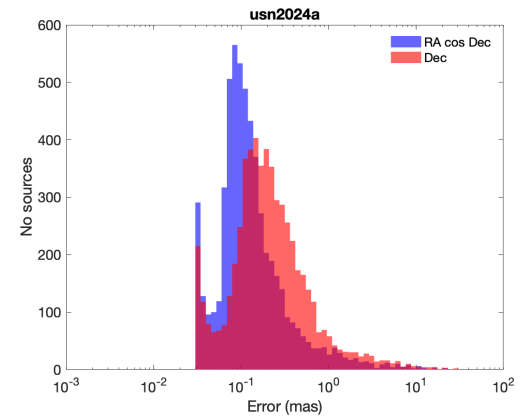
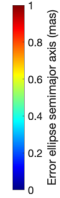
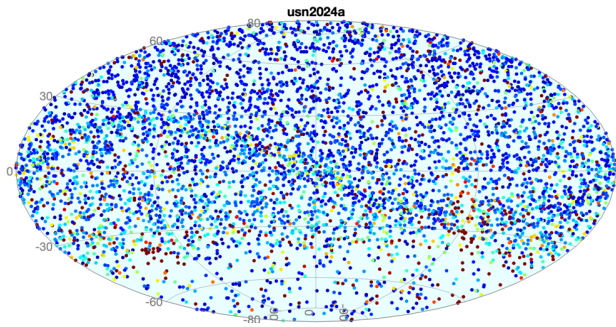
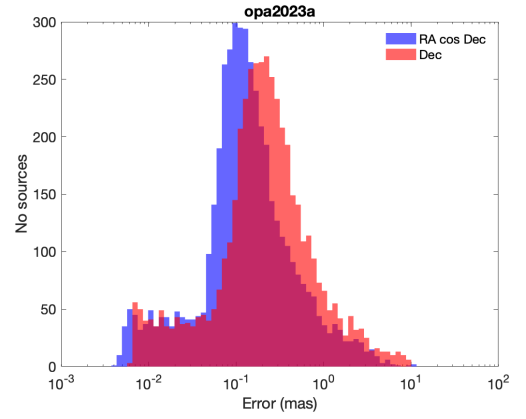
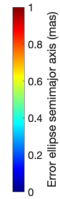
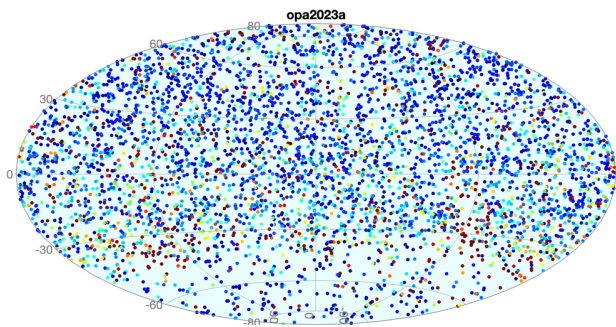


Figure 1 – Previous pages. *Left: sky distribution of the catalogs highlighting the overall positional error computed as the major axis of the error ellipse. Right: distribution of the standard errors on source position.*

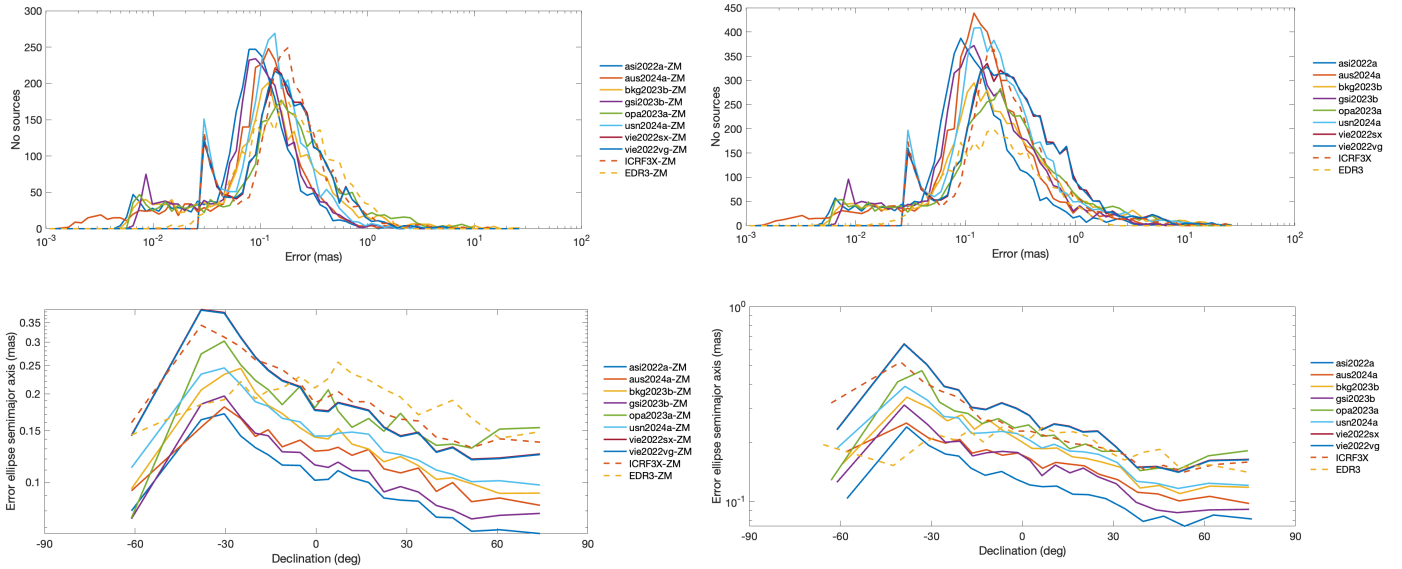


Figure 2. *Top: overall comparison of the standard error distribution for sources common to all catalogs (left) and for all sources in each catalog (right). Bottom: standard errors in source positions as a function of the declination smoothed by taking the running median within bins of 15 degrees, for sources common to all catalogs (left) and for all sources in each catalog (right).*

Figure 2 presents four plots; at the top the error distribution, including that of the catalogs used as reference in the comparisons (ICRF3X and Gaia EDR3) for sources common to all catalogs on the left and for all sources in each catalog on the right; at the bottom the dependence of the error (considering the value of the semimajor axis of the error ellipse) on the declination including the common sources to all catalogs (left) and all sources in each catalog (right) are displayed for which we took the running median error within windows of 15°.

A clear dependence of the error on the declination is visible for all catalogs. The behavior of the VLBI solutions is similar, both for sources common to all catalogs and for all sources in each individual catalogs, peaking at about -40° declination, and reaching small error values around +60° declination, certainly due to the presence of a substantial number of good astrometric common sources in that region. When all sources in each catalog are considered, the errors are slightly larger. The Gaia scanning law allows to cover both hemispheres symmetrically, and in consequence the Gaia EDR3 catalog does not show such systematic effects, as ICRF3 does.

3.3. Comparison with ICRF3 and Gaia EDR3

Figures 3 and 4 display the differences in declination between the catalogs and the references averaged within bins of 200 sources in two configurations: sources common to all catalogs (top) and all sources (bottom). In the comparison with ICRF3X presented in Figure 3, common sources, the USN and GSI solutions are rather smooth, particularly above 0° declination, with some deformations of about -40 μas between 0° and -30° declination. The solutions of VIE and BKG show a similar trend at positive

declinations, and peak down to $-70 \mu\text{s}$ and $-80 \mu\text{s}$ at declinations between -30° and 0° . OPA solution is rather erratic, peaking up and down in the range $20 \mu\text{s}$ to $-50 \mu\text{s}$ at several declinations. Deformations are smoother when the differences are computed with all common sources.

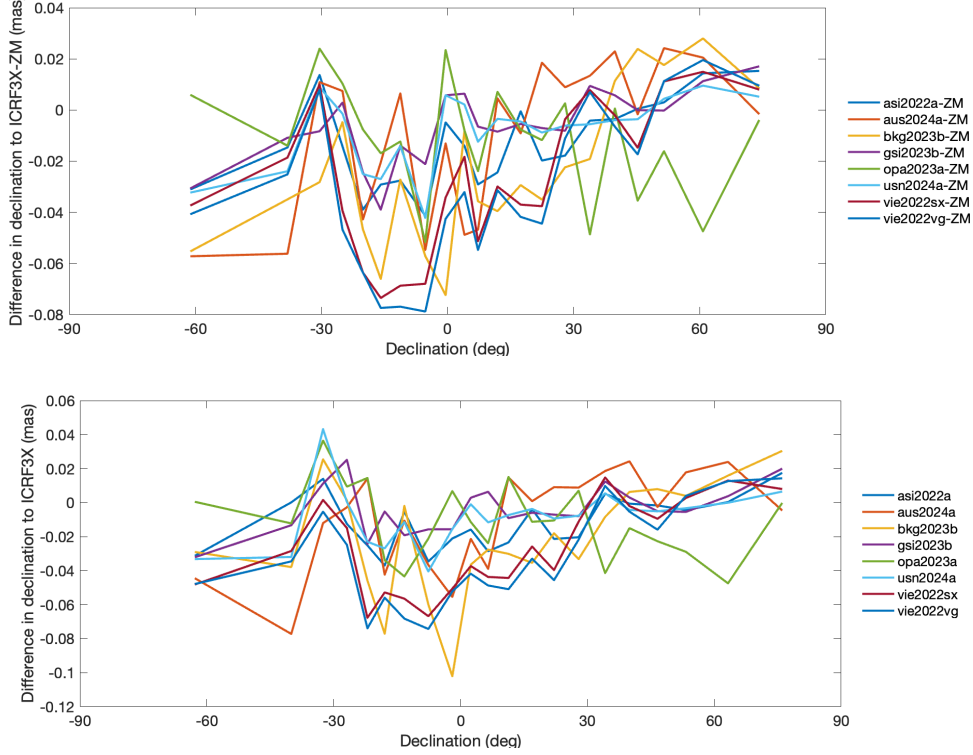


Figure 3. Differences in declination between the catalogs and ICRF3X, averaged in bins of 200 sources sorted by declination for common sources to all catalogs (top) and sources common to the pair in the comparison (bottom).

The comparisons with respect to Gaia EDR3 are presented in Figure 4. Since the sphere of Gaia is in principle not affected by deformations, the amplitude of the zonal deformations of the VLBI solutions is large, ranging between $-180 \mu\text{s}$ and $120 \mu\text{s}$ south from -30° declination. All solutions show similar behavior.

Catalog comparisons had been computed using the 16-parameter transformation accounting for rotations around the three axes, a glide, and degree-2 electric- and magnetic-type deformations (see e.g., Mignard and Klioner 2012) together with an outlier elimination process preliminary to the fit as described in Charlot et al. (2020). The coordinate differences $\Delta\alpha$ and $\Delta\delta$ between a catalog and a reference catalog read

$$\begin{aligned}
 \Delta\alpha \cos \delta &= R_1 \cos \alpha \sin \delta + R_2 \sin \alpha \sin \delta - R_3 \cos \delta - D_1 \sin \alpha + D_2 \cos \alpha + M_{20} \sin 2\delta \\
 &+ (E_{21}^{\text{Re}} \sin \alpha + E_{21}^{\text{Im}} \cos \alpha) \sin \delta - (M_{21}^{\text{Re}} \cos \alpha - M_{21}^{\text{Im}} \sin \alpha) \cos 2\delta \\
 &- 2 (E_{22}^{\text{Re}} \sin 2\alpha + E_{22}^{\text{Im}} \cos 2\alpha) \cos \delta - (M_{22}^{\text{Re}} \cos 2\alpha - M_{22}^{\text{Im}} \sin 2\alpha) \sin 2\delta, \\
 \Delta\delta &= -R_1 \sin \alpha + R_2 \cos \alpha - D_1 \cos \alpha \sin \delta - D_2 \sin \alpha \sin \delta + D_3 \cos \delta + E_{20} \sin 2\delta \\
 &- (E_{21}^{\text{Re}} \cos \alpha - E_{21}^{\text{Im}} \sin \alpha) \cos 2\delta - (M_{21}^{\text{Re}} \sin \alpha + M_{21}^{\text{Im}} \cos \alpha) \sin \delta \\
 &- (E_{22}^{\text{Re}} \cos 2\alpha - E_{22}^{\text{Im}} \sin 2\alpha) \sin 2\delta + 2 (M_{22}^{\text{Re}} \sin 2\alpha + M_{22}^{\text{Im}} \cos 2\alpha) \cos \delta,
 \end{aligned}$$

where α and δ are the coordinates of the object in the reference catalog. We used weighted least-squares to solve the system, with weights computed using the available covariance information (i.e., the standard errors on individual source coordinates and their correlation). The values of the transformation parameters adjusted to the catalogs compared to the ICRF3X and Gaia EDR3 and their standard errors are reported in Figures 5 and 6 for two different set of sources, those common to all catalogs and each reference, and those common between each catalog and the reference. The resulting statistics after removal of systematics are reported in Table 2. The figures reveal that the results are similar independently from the set of sources used for the comparisons. The comparison with ICRF3X in Figure 5 shows significant rotation parameters for OP and BKG solutions. The parameter D3, representing a deformation in declination is significant in general, and particularly large for the GSI and VIE solutions. Deformations are also visible through the glide parameters. The rotation effects are also visible when Gaia EDR3 is the reference (Figure 6), since it has been oriented onto ICRF3. Deformations are visible dependent on declination, consistently with Fig. 2.

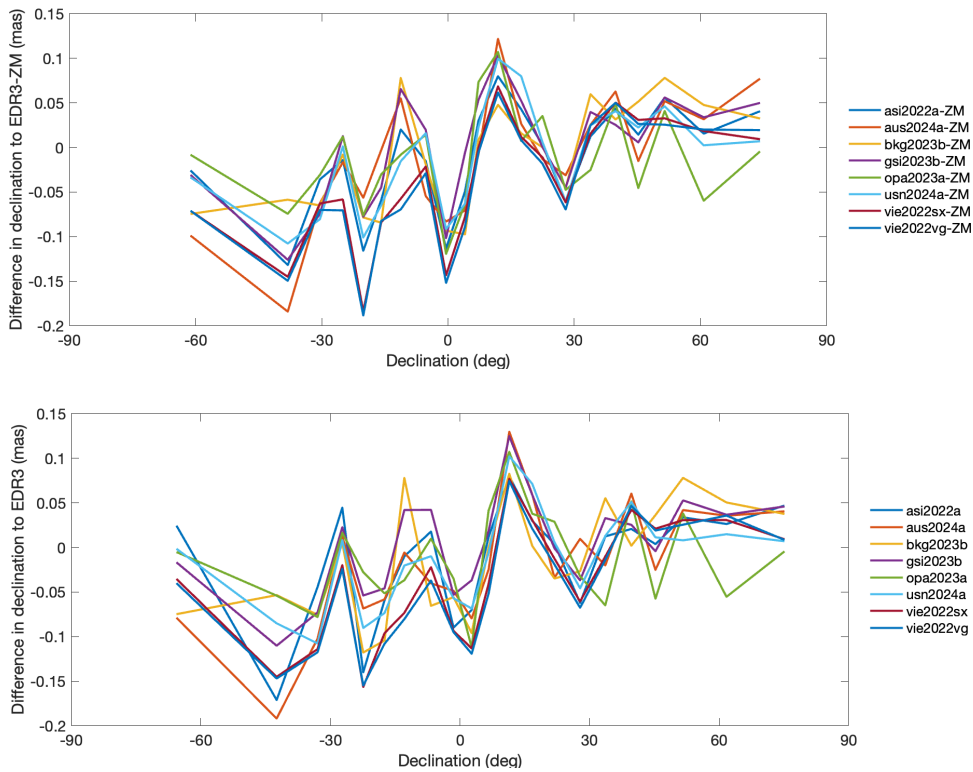


Figure 4. Differences in declination between the catalogs and Gaia EDR3, averaged in bins of 200 sources sorted by declination for common sources to all catalogs (top) and sources common to the pair in the comparison (bottom).

Galactic aberration has been accounted for at the construction of ICRF3. Uncorrected Galactic aberration should provoke a glide of amplitude close to $5 \mu\text{s/yr}$ (e.g., Kovalevsky 2003; Titov et al. 2011) towards the Galactic center (approx. R.A. 265° and declination -29°). A value of $5.8 \mu\text{s/yr}$ for the amplitude of the Galactic aberration has been evaluated in analyses performed at the construction of the ICRF3 (MacMillan et al. 2019). The descriptions of the catalogs provided to the IVS used in this report indicate that this correction has been applied in the solutions (for details refer to <http://ivsopar.obspm.fr/vlbi/ivsproducts/crf/>).

Table 2. Statistics of the differences of the catalogs to ICRF3X and Gaia EDR3 with sources common to each pair of catalogs compared, before transformation and after removal of large-scale systematics. RA* stands for RA cos_dec. Unit is μas .

Comparison against ICRF3X													
		----- Before transformation -----						----- After transformation -----					
		Std_RA*	Std_Dec	Chi2	Chi2	MAD_RA*	MAD_Dec	Std_RA*	Std_Dec	Chi2	Chi2	MAD_RA*	MAD_Dec
		uas	uas	RA*	Dec	uas	uas	uas	uas	RA*	Dec	uas	uas
N													
asi2022a	4362	89.18	177.81	1.07	2.95	64.04	100.70	88.66	177.26	1.06	2.93	62.88	99.14
aus2024a	4164	150.61	201.00	2.81	3.49	128.51	216.55	150.65	200.25	2.82	3.46	128.64	214.77
bkg2023b	3913	7723.75	749.67	7643.86	50.73	107.20	172.75	7723.66	747.80	7643.68	50.48	102.40	166.33
gsi2023b	4437	85.73	158.96	0.96	2.30	64.68	98.35	84.67	157.85	0.93	2.27	62.49	97.78
opa2023a	4168	161.63	224.39	3.21	4.53	75.25	125.10	159.00	217.62	3.11	4.26	68.88	117.18
usn2024a	4438	105.61	158.95	0.94	1.44	61.13	94.90	105.17	158.28	0.93	1.43	59.43	95.42
vie2022sx	4423	114.40	227.96	0.99	2.70	72.39	115.90	113.82	226.71	0.98	2.67	71.14	114.61
vie2022vg	4420	116.68	228.02	1.04	2.72	72.48	114.70	115.91	226.93	1.02	2.69	72.40	113.78

Comparison gainst EDR3													
		----- Before transformation -----						----- After transformation -----					
		Std_RA*	Std_Dec	Chi2	Chi2	MAD_RA*	MAD_Dec	Std_RA*	Std_Dec	Chi2	Chi2	MAD_RA*	MAD_Dec
		uas	uas	RA*	Dec	uas	uas	uas	uas	RA*	Dec	uas	uas
N													
asi2022a	2541	1823.67	1787.78	247.43	201.33	252.54	282.40	1823.49	1787.50	247.38	201.26	252.03	284.67
aus2024a	2404	1952.40	1872.37	238.06	178.81	286.53	361.80	1952.26	1872.04	238.02	178.75	287.31	356.66
bkg2023b	2395	13995.58	2013.16	12007.62	217.67	285.75	351.35	13995.41	2011.98	12007.34	217.42	288.44	350.97
gsi2023b	2601	1883.52	1929.30	245.61	220.60	259.28	291.00	1883.40	1928.89	245.58	220.51	255.97	291.33
opa2023a	2522	1605.99	1841.99	152.21	178.28	308.94	358.00	1605.39	1841.59	152.10	178.20	304.64	349.74
usn2024a	2674	2078.52	2183.96	193.79	177.25	253.20	286.40	2078.44	2183.92	193.77	177.25	254.80	282.44
vie2022sx	2705	1987.74	2168.70	152.75	148.36	259.59	279.60	1987.55	2168.57	152.72	148.34	255.81	280.85
vie2022vg	2705	1985.73	2165.44	153.23	148.73	259.17	281.90	1985.55	2165.36	153.21	148.72	257.09	281.24

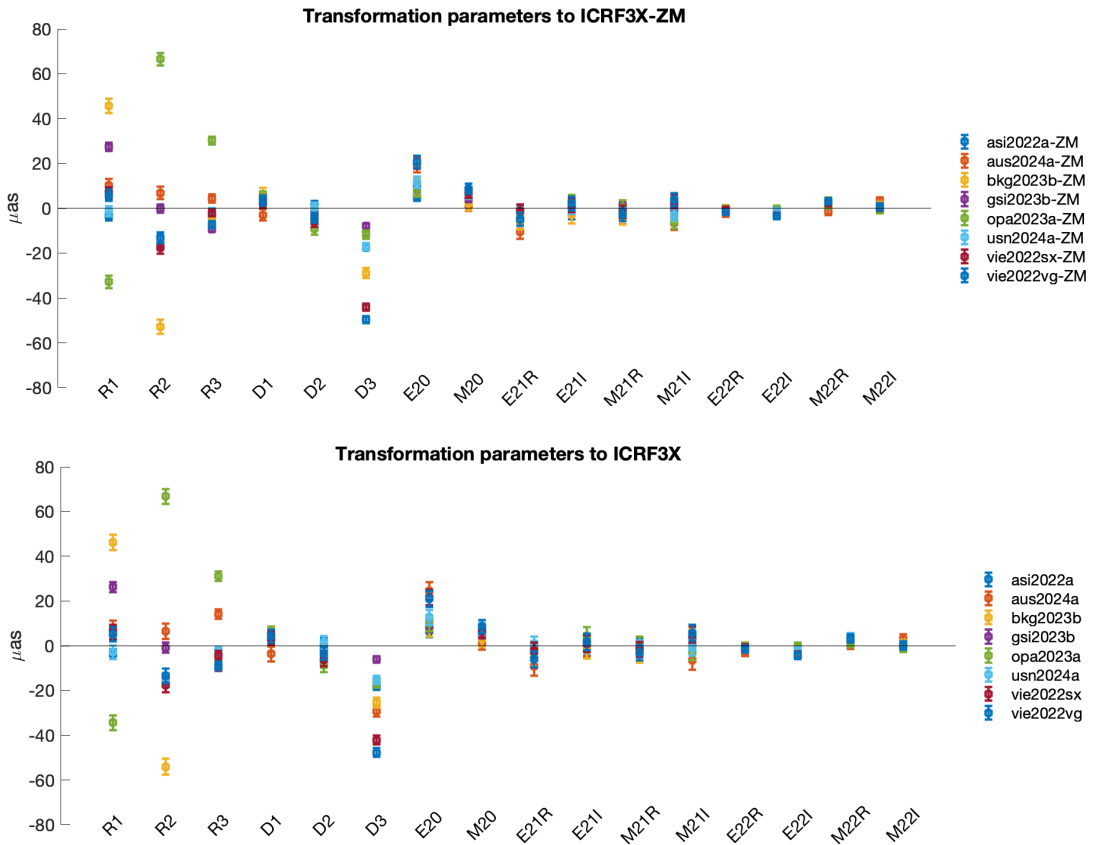


Figure 5. Transformation parameters between the catalogs under analysis and ICRF3X. The plot on top represents parameters computed with sources common to all the catalogs involved in the comparisons, including the references; the plot at the bottom represents parameters computed with sources common to each individual catalog and the frame used as reference. They correspond to the statistics in table 2 (top).

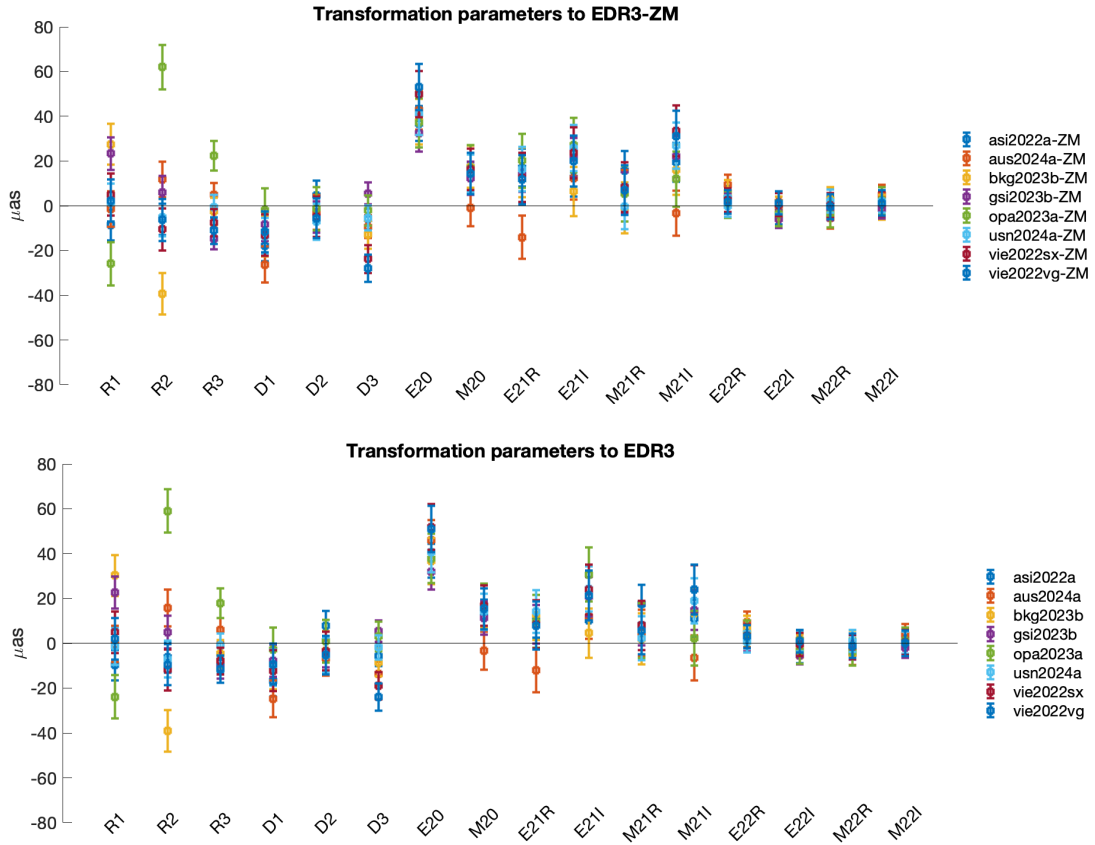


Figure 6. Transformation parameters between the catalogs under analysis and Gaia EDR3. The plot on top represent parameters computed with sources common to all the catalogs involved in the comparisons, including the references; the plot at the bottom represents parameters computed with sources common to each individual catalog and the frame used as reference. They correspond to the statistics in table 2 (bottom).

3.4. Conclusions and recommendations

Eight individual catalogs from four analysis centres computed in 2022, 2023 and 2024 are analyzed in this report. The axes of their frames are consistent with ICRF3X at the level of $10 \mu\text{as}$ for most solutions, with misalignments of $-60 \mu\text{as}$, $70 \mu\text{as}$ in two cases (OP and BKG). Zonal deformation remains in general beyond $20 \mu\text{as}$, but catalog equators are shifted up to $-50 \mu\text{as}$ in VIE solutions. Rotations are observed in the comparisons with Gaia EDR3, and significant zonal deformations.

In all solutions the correction for the amplitude of the Galactic aberration has been implemented using the recommended value. The catalogs should be as complete as possible, i.e., processing as much VLBI sessions as possible since 1979. Analysis strategies should be rigorously documented and motivated. The main points that will be scrutinized in the next reports will be the zonal systematics, their relation with the Galactic aberration, and the agreement with the current (EDR3) and future releases of Gaia.

4. References

- J. Boehm, S. Boehm, J. Boisits, A. Girdiuk, J. Gruber, A. Hellerschmied, H. Krásná, Landskron, M. Madzak, D. Mayer, J. McCallum, L. McCallum, M. Scherter and K. Teke. Vienna VLBI and Satellite Software (VieVS) for Geodesy and Astrometry. PASP 130 044503, 2018.
- A. G. A. Brown, A. Vallenari, T. Prusti, J. H. J. de Bruijne, et al. Gaia Data Release 1. Summary of the astrometric, photometric, and survey properties. *Astronomy & Astrophysics*, 595:A2, Nov. 2016.
- A. G. A. Brown, A. Vallenari, T. Prusti, J. H. J. de Bruijne, et al. Gaia Data Release 2. Summary of the contents and survey properties. *Astronomy & Astrophysics*, 616:A1, Aug. 2018.
- A. G. A. Brown, A. Vallenari, T. Prusti, J. H. J. de Bruijne, et al. Gaia Early Data Release 3. Summary of the contents and survey properties. *Astronomy & Astrophysics*, 649:A1, 2021.
- P. Charlot, C. S. Jacobs, D. Gordon, S. B. Lambert, A. de Witt, J. Boehm, A. L. Fey, R. Heinkelmann, E. Skurikhina, O. Titov, E. F. Arias, S. Bolotin, G. Bourda, C. Ma, Z. Malkin, A. Nothnagel, D. Mayer, D. S. MacMillan, T. Nilsson and R. Gaume, The third realization of the International Celestial Reference Frame by very long baseline interferometry. *Astronomy & Astrophysics*, 644, A159, Dec. 2020.
- International Astronomical Union. Transactions IAU, Vol. XXXB, Proc. of the XXX IAU General Assembly, August 2018 (Ed. Teresa Lago), 2019.
- S. A. Klioner, L. Lindegren, F. Mignard, J. Hernandez, et al. Gaia Early Data Release 3. The celestial reference frame (Gaia-CRF3). *Astronomy & Astrophysics*, 2022.
- J. Kovalevsky. Aberration in proper motions. *Astronomy & Astrophysics*, 404:743–747, June 2003.
- S. Lambert, Z. Malkin. Estimation of large-scale deformations in VLBI radio source catalogs with mitigation of impact of outliers: a comparison between different L1- and L2-norm-based methods, *Astronomy and Astrophysics*, 669, 138, 2023
- C. Ma, T. A. Clark, J. W. Ryan, T. A. Herring, I. I. Shapiro, B. E. Corey, H. F. Hinteregger, A. E. E. Rogers, A. R. Whitney, C. A. Knight, G. L. Lundqvist, D. B. Shaffer, N. R. Vandenberg, J. C. Pigg, B. R. Schupler, and B. O. Ronnang. Radio-source positions from VLBI. *Astronomical Journal*, 92:1020–1029, Nov. 1986.
- D. S. MacMillan, A. L. Fey, J. M. Gipson, D. Gordon, C. S. Jacobs, H. Krásná, S. Lambert, Z. Malkin, O. A. Titov, G. Wang, and M. H. Xu, Galactocentric acceleration in VLBI analysis - Findings of IVS WG8, *Astronomy and Astrophysics*, 630:A93, 2019
- F. Mignard and S. Klioner. Analysis of astrometric catalogues with vector spherical harmonics. *Astronomy & Astrophysics*, 547:A59, 2012.
- F. Mignard, S. A. Klioner, L. Lindegren, J. Hernández, U. Bastian, A. Bombrun, D. Hobbs, U. Lammers, D. Michalik, and et al. Gaia Data Release 2. The celestial reference frame (Gaia-CRF2). *Astronomy & Astrophysics*, 616:A14, 2018.

T. Prusti, J. H. J. de Bruijne, A. G. A. Brown, Vallenari, A., Babusiaux, C., Bailer-Jones, C. A. L., Bastian, U., Biermann, M., Evans, D. W., and et al. The Gaia mission. *Astronomy & Astrophysics*, 595:A1, 2016.

O. Titov, V. Tesmer, and J. Boehm. OCCAM v.6.0 Software for VLBI Data Analysis. In N. R. Vandenberg and K. D. Baver, editors, *International VLBI Service for Geodesy and Astrometry 2004 General Meeting Proceedings*, page 267, June 2004.

O. Titov, S. B. Lambert, and A.-M. Gontier. VLBI measurement of the secular aberration drift. *Astronomy & Astrophysics*, 529:A91, May 2011.